International Journal of Pressure Vessels and Piping 98 (2012) 119–128

Contents lists available at SciVerse ScienceDirect

International Journal of Pressure Vessels and Piping

journal homepage: www.elsevier.com/locate/ijpvp

Free vibrations and buckling analysis of carbon nanotube-reinforced composite Timoshenko beams on elastic foundation

M.H. Yas*, N. Samadi

Mech. Eng. Department, Razi University, Kermanshah, Iran

ARTICLE INFO

Article history:
Received 30 April 2012
Received in revised form
24 July 2012
Accepted 25 July 2012

Keywords:
Carbon nanotube
Timoshenko beam
Elastic foundation
Free vibrations
Buckling load

ABSTRACT

This study deals with free vibrations and buckling analysis of nanocomposite Timoshenko beams reinforced by single-walled carbon nanotubes (SWCNTs) resting on an elastic foundation. The SWCNTs are assumed to be aligned and straight with a uniform layout. Four different carbon nanotubes (CNTs) distributions including uniform and three types of functionally graded distributions of CNTs through the thickness are considered. The rule of mixture is used to describe the effective material properties of the nanocomposite beams. The governing equations are derived through using Hamilton's principle and then solved by using the generalized differential quadrature method (GDQM). Natural frequencies and critical buckling load are obtained for nanocomposite beams with different boundary conditions. Effects of several parameters, such as nanotube volume fraction, foundation stiffness parameters, slenderness ratios, CNTs distribution and boundary conditions on both natural frequency and critical buckling load are investigated. The results indicate that the above-mentioned parameters play a very important role on the free vibrations and buckling characteristics of the beam.

1. Introduction

Exceptional electronic and mechanical properties of carbon nanotubes, such as the extremely high elastic modulus, tensile strength, aspect ratio and low density, make them excellent candidate for the reinforcement of polymer composites [1–4]. The mechanical properties of carbon nanotube reinforced composites (CNTRCs) have been extensively investigated experimentally, analytically and numerically. Hu et al. [5] evaluated the macroscopic elastic properties of carbon nanotube-reinforced composites through analyzing the elastic deformation of a representative volume element under various loading conditions. Using molecular dynamics (MD), Han and Elliott [6] simulated the elastic properties of polymer/carbon nanotube composites. Wan et al. [7] investigated the effective moduli of the CNT reinforced polymer composite, with emphasis on the influence of CNT length and CNT-matrix interphase on the stiffening of the composite. These researches demonstrated that the incorporation of nanotubes in the polymer matrices can lead to significant enhancements in the composite properties even at very low volume fractions of CNTs. In actual structural applications, CNTRCs, as a type of advanced material, may be incorporated in the forms of beams, plates or shells as structural components. It is thus important to explore mechanical responses of the structures made of CNTRC. Wuite and Adali [8] found that the stiffness of CNTRC beams can be improved significantly by the homogeneous dispersion of a small percentage of CNTs. Vodenitcharova and Zhang [9] investigated the pure bending and bending-induced local buckling of CNTRC beams. However, the experimental and numerical studies concerning CNTRCs have shown that distributing CNTs uniformly as the reinforcements in the matrix can only achieve moderate improvement of the mechanical properties [10,11]. This is mainly due to the weak interface between the CNTs and the matrix where a significant material property mismatch exists.

Shen [12] for the first time suggested that the nonlinear bending behavior of CNTRC plates can be considerably improved through the use of a functionally graded distribution of CNTs in the matrix. Functionally graded materials (FGMs) are inhomogeneous composites characterized by smooth and continuous variations in both compositional profile and material properties and have found a wide range of applications in many industries [13–15]. Reviewing the literature on FG-CNTRC, it is inferred that the literature is mostly devoted to analysis of plates and shells made of FG-CNTRC and relatively very few research works have been done on CNTRC beams [16–22]. Ke et al. [23] analyzed the nonlinear free vibrations of FG-CNTRC Timoshenko beams with symmetric and

* Corresponding author. Prof. of Solid Mech, Mech. Eng. Dept., Razi University, Kermanshah, Iran.
E-mail address: yas@razi.ac.ir (M.H. Yas).

0308-0161/$ – see front matter © 2012 Elsevier Ltd. All rights reserved.
http://dx.doi.org/10.1016/j.ijpvp.2012.07.012

Nomenclature

$E_{11}^{cnt}, E_{22}^{cnt}, E^m$	elastic moduli for CNT and matrix
E_{11},E_{22}	elastic moduli for a nanocomposite
G_{12}^{cnt}, G^m	shear modulus for carbon nanotube and matrix
V_{cnt} , V_m	volume fractions of carbon nanotube and matrix
W_{cnt}	mass fraction of carbon nanotube
η_i	carbon nanotube efficiency parameteres
U, W	axial displacement and transverse deflection
$u_0, w_0, \overline{U}, \overline{W}$	axial displacement and transverse deflection of any point in the mid-surface and their dimensionless forms
L,b,h	length, width and height of the beam
x,z,t,ξ,z,τ	cartesian coordinate variables, time and their dimensionless forms
σ_{xx},τ_{xz}	normal stress and shear stress
A_{11},B_{11},D_{11},A_{55}	beam stiffness components
a_{11},b_{11},d_{11},a_{55}	dimensionless beam stiffness components
I_1,I_2,I_3	inertia terms
$\overline{I}_1, \overline{I}_2, \overline{I}_3$	dimensionless inertia terms
KW, K_S, k_w, k_s	Winkler and shearing layer elastic coefficients of foundation and their dimensionless forms
ω,P	dimensionless natural frequency and critical buckling load
N	number of grid points
A_{ij},B_{ij}	the weighting coefficients for the first and second order derivative

unsymmetrical distributions of CNTs along the thickness direction using Ritz method and direct iterative technique. Recently, Yas and heshmati [24] investigated dynamic analysis of functionally graded nanocomposite beams reinforced by randomly oriented carbon nanotube under the action of moving load by using Euler–Bernoulli and Timoshenko beam theories and based on the Eshelby–Mori–Tanaka approach.

This study presents the free vibrations and buckling analysis of nanocomposite beams resting on elastic foundation. The nanocomposite beam is reinforced by the SWCNT and has different boundary conditions. The CNTs are assumed to be uniformly or functionally graded distributed through the thickness direction and the material properties are estimated through a micromechanical model in which the CNT efficiency parameter is estimated by matching the elastic modulus of CNTRCs observed from the molecular dynamics (MD) simulation results with the numerical results obtained from the rule of mixture. Theoretical formulations based on Timoshenko beam theory are used to account transverse shear deformation and rotary inertia. The generalized differential quadrature method is used to solve the governing equations of motion to obtain the natural frequencies and critical buckling load of the CNTRC beams. One important parameter in the design of composite pressure vessels and piping reinforced with CNTs is to find and select suitable distribution of CNTs for maximum natural frequency or critical buckling load. In this study we considered this issue and found the effect of different types of CNTs distributions for beam structure which can be extended for pressure vessels too.

2. Material properties of CNTRC beams

The uniform distribution (UD) and functionally graded distributions (FG–Λ, FG–◇ and FG–X) of carbon nanotubes in the thickness direction of the composite beams (z axis direction) are shown in Fig. 1. In this figure the density of CNTs within the area is constant and the volume fraction varies through the thickness of the beam. We used an embedded carbon nanotube in a polymer matrix. Thus there is no abrupt interface between the CNT and polymer matrix in the entire region of the beam. It is assumed the CNTRC beams are made of a mixture of SWCNTs and an isotropic matrix. The rule of mixture is employed to estimate the effective material properties of CNTRC beams. According to rule of mixture model the effective Young's modulus and shear modulus of CNTRC beams can be expressed as [12]

$$E_{11} = \eta_1 V_{cnt} E_{11}^{cnt} + V_m E^m \tag{1a}$$

$$\frac{\eta_2}{E_{22}} = \frac{V_{cnt}}{E_{22}^{cnt}} + \frac{V_m}{E^m} \tag{1b}$$

$$\frac{\eta_3}{G_{12}} = \frac{V_{cnt}}{G_{12}^{cnt}} + \frac{V_m}{G^m} \tag{1c}$$

where E_{11}^{cnt}, E_{22}^{cnt} and G_{12}^{cnt} indicate the Young's moduli and shear modulus of SWCNTs, respectively. E^m and G^m represent the corresponding properties of the isotropic matrix. The CNT efficiency parameters $\eta_i (i = 1,2,3)$, are introduced in Eq. (1) to consider the size-dependent material properties and will be calculated later by matching the elastic moduli of CNTRCs predicted by the MD simulations with the numerical results obtained from the rule of mixture. V_{cnt} and V_m are the volume fractions for carbon nanotube and matrix respectively which are related by $V_m + V_{cnt} = 1$. Similarly, Poisson's ratio υ and mass density ρ of the CNTRC beams can be expressed as:

$$\upsilon = V_{cnt}\upsilon^{cnt} + V_m\upsilon^m \quad , \quad \rho = V_{cnt}\rho^{cnt} + V_m\rho^m \tag{2}$$

where υ^{cnt},υ^m are the Poisson's ratios, and ρ^{cnt},ρ^m are the densities of the CNT and matrix, respectively. The different distributions of the carbon nanotubes along the thickness direction of the nanocomposite beams depicted in Fig. 1 are assumed to be as follows:

$$\text{UD}-: \quad V_{cnt} = V_{cnt}^* \tag{3}$$

$$\text{FG}-\Lambda: \quad V_{cnt} = \left(1 + \frac{2z}{h}\right) V_{cnt}^* \tag{4}$$

$$\text{FG}-\text{X}: \quad V_{cnt} = 4\frac{|z|}{h} V_{cnt}^* \tag{5}$$

$$\text{FG}-\diamond: \quad V_{cnt} = 2 - 4\frac{|z|}{h} V_{cnt}^* \tag{6}$$

where V_{cnt}^* is the volume fraction of CNTs that is calculated from:

$$V_{cnt}^* = \frac{W_{cnt}}{W_{cnt} + (\rho^{cnt}/\rho^m)(1 - W_{cnt})} \tag{7}$$

W_{cnt} is the mass fraction of CNTs

3. Theory and formulations

3.1. Equations of motion

The analyzed physical system is a CNTRC beam of length L, width b, thickness h, with arbitrary boundary conditions along the $x = 0$ and L edges, as shown in Fig. 2. The beam is resting on an elastic foundation whose supporting action is described by Pasternak-type relationship $p = K_w W - K_s \frac{\partial^2 W}{\partial x^2}$, in which p is the foundation

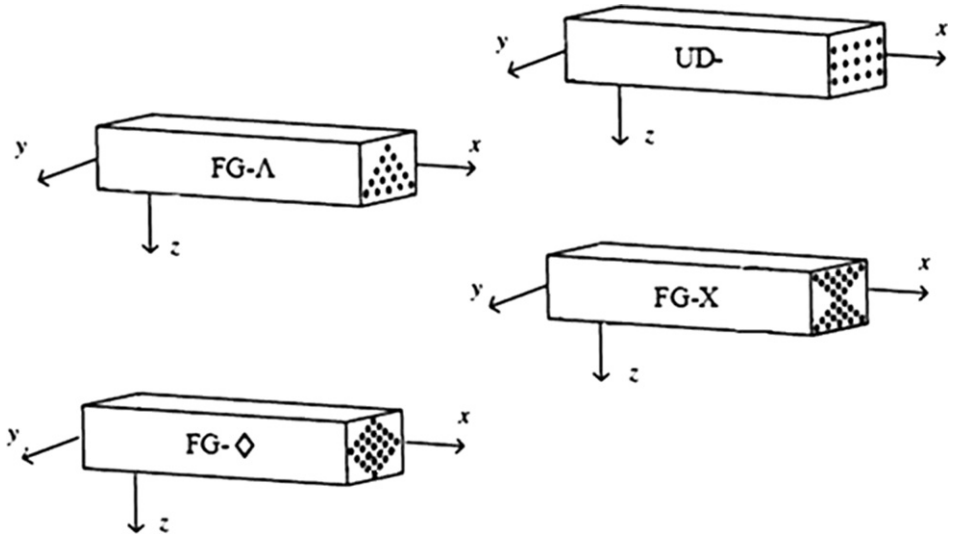

Fig. 1. Configurations of the carbon nanotube-reinforced composite beams.

reaction per unit area, W is the transverse deflection of the beam, K_w and K_s are Winkler and shearing layer elastic coefficients of the foundation. When $K_s = 0$, the foundation model reduces to Winkler type. According to Timoshenko beam theory, the displacements of any point in the beam along the x- and z-axes, denoted by $U(x, z, t)$ and $W(x, z, t)$ respectively as follows [25]:

$$U(x,z,t) = u_0(x,t) + z\Psi(x,t), \quad W(x,z,t) = w_0(x,t) \tag{8}$$

where u_0 and w_0 are displacement components at the mid-surface of the beam, also Ψ is the section normal vector rotations about the y-, and t denotes time. The linear normal strain ε_x and shear strain γ_{xz} are associated with the displacements via

$$\varepsilon_x = \frac{\mathrm{d}u_0}{\mathrm{d}x} + z\frac{\mathrm{d}\Psi}{\mathrm{d}x}, \quad \gamma_{xz} = \frac{\mathrm{d}w_0}{\mathrm{d}x} + \Psi \tag{9}$$

The normal stress σ_{xx} and shear stress τ_{xz} are given by linear elastic constitutive law as:

$$\sigma_x = Q_{11}(z)\varepsilon_x, \quad \tau_{xz} = Q_{55}(z)\gamma_{xz} \tag{10}$$

where

$$Q_{11}(z) = \frac{E(z)}{1-\nu^2(z)}, \quad Q_{55}(z) = G_{12}(z) \tag{11}$$

The governing differential equations of motion and the related boundary conditions can be derived from Hamilton's principle.

$$\delta\int_0^t (T - \Pi + \Upsilon_p)\mathrm{d}t = 0 \tag{12}$$

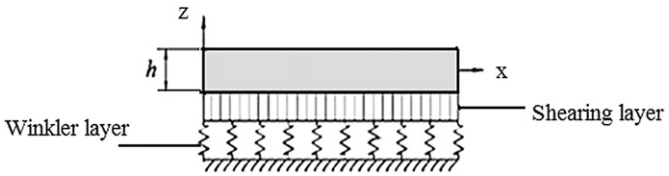

Fig. 2. Geometry of a CNTRC beam.

where δ represents the variational symbol, T is the kinetic energy of the beam, Π is the potential energy composed of strain energy of the beam together with the elastic potential energy of the elastic foundation, and Υ_p is the work done by the axial force N_{x0}

$$\begin{aligned} T &= \frac{b}{2}\int_0^L\int_{-h/2}^{h/2} \rho(z)\left[\left(\frac{\partial U}{\partial t}\right)^2 + \left(\frac{\partial W}{\partial t}\right)^2\right]\mathrm{d}z\mathrm{d}x \\ \Pi &= \frac{b}{2}\int_0^L\int_{-h/2}^{h/2} (\sigma_x\varepsilon_x + \tau_{xz}\gamma_{xz})\mathrm{d}z\,\mathrm{d}x + \frac{b}{2}\int_0^L\left[K_w W^2 + K_s\left(\frac{\partial W}{\partial x}\right)^2\right]\mathrm{d}x \\ \Upsilon_p &= \frac{b}{2}\int_0^L\left[N_{x0}\left(\frac{\partial W}{\partial x}\right)^2\right]\mathrm{d}x \end{aligned} \tag{13}$$

Substituting Eq. (13) into the virtual work statement in Eq. (12) and integrating trough the beam thickness and then setting the coefficients of δu, δw and $\delta\Psi$ to zero lead to the equations of motion as

$$\begin{aligned} \delta u &: \frac{\partial N_x}{\partial x} = I_1\frac{\partial^2 u_0}{\partial t^2} + I_2\frac{\partial^2\Psi}{\partial t^2} \\ \delta w &: \frac{\partial Q_x}{\partial x} - K_f w + K_s\frac{\partial^2 w_0}{\partial x^2} + N_{x0}\frac{\partial^2 w_0}{\partial x^2} = I_1\frac{\partial^2 w_0}{\partial t^2} \\ \delta\Psi &: \frac{\partial M_x}{\partial x} - Q_x = I_2\frac{\partial^2 u_0}{\partial t^2} + I_3\frac{\partial^2\Psi}{\partial t^2} \end{aligned} \tag{14}$$

axial force N_x, bending moment M_x and shear force Q_x are stress resultant, which can be defined as:

$$\begin{Bmatrix} N_x \\ M_x \\ Q_x \end{Bmatrix} = \int_{-h/2}^{h/2} \begin{Bmatrix} \sigma_{xx} \\ z\sigma_{xx} \\ \tau_{xz} \end{Bmatrix}\mathrm{d}z \tag{15}$$

Substituting Eqs. (9) and (10) into Eq. (15) yields,

$$N_x = A_{11}\frac{\partial u_0}{\partial x} + B_{11}\frac{\partial \Psi}{\partial x}$$
$$M_x = B_{11}\frac{\partial u_0}{\partial x} + D_{11}\frac{\partial \Psi}{\partial x} \tag{16}$$
$$Q_x = \kappa A_{55}\left(\frac{\partial w_0}{\partial x} + \Psi\right)$$

κ denotes the shear modification coefficient and is taken $\kappa = 5/6$ in this paper, the stiffness components and inertia terms are calculated by:

$$(A_{11}, B_{11}, D_{11}) = \int_0^L Q_{11}(z)\left(1, z, z^2\right)\mathrm{d}z, \quad A_{55} = \int_{-h/2}^{h/2} Q_{55}(z)\mathrm{d}z$$
$$(I_1, I_2, I_3) = \int_0^L \rho(z)(1, z, z^2)\mathrm{d}z \tag{17}$$

Substituting Eq. (16) into Eq. (14) leads to the following differential equations of motion:

$$A_{11}\frac{\partial^2 u_0}{\partial x^2} + B_{11}\frac{\partial^2 \Psi}{dx^2} = I_1\frac{\partial^2 u_0}{\partial t^2} + I_2\frac{\partial^2 \Psi}{\partial t^2}$$
$$\kappa A_{55}\left(\frac{\partial^2 w_0}{\partial x^2} + \frac{\partial \Psi}{\partial x}\right) - K_w w_0 + K_s\frac{\partial^2 w_0}{\partial x^2} + N_{x0}\frac{\partial^2 w_0}{\partial x^2} = I_1\frac{\partial^2 w_0}{\partial t^2}$$
$$B_{11}\frac{\partial^2 u_0}{\partial x^2} + D_{11}\frac{\partial^2 \Psi}{\partial x^2} - \kappa A_{55}\left(\frac{\partial w_0}{\partial x} + \Psi\right) = I_2\frac{\partial^2 u_0}{\partial t^2} + I_3\frac{\partial^2 \Psi}{\partial t^2} \tag{18}$$

In this investigation different boundary conditions of the beams such as hinged–hinged (H–H), clamped-hinged (C–H), clamped–clamped (C–C), clamped-free (C–F) are considered. These conditions are described as:

$$\begin{aligned}&\text{Clamped(C):} \quad u_0 = w_0 = \Psi = 0\\ &\text{Hinged(H):} \quad u_0 = w_0 = M_x = 0\\ &\text{Free(F):} \quad N_x = Q_x + N_{x0}\frac{\partial w_0}{\partial x} = 0 \quad M_x = 0\end{aligned} \tag{19}$$

In this study we used beam with hinged condition over simply supported beam, because we need to compare our results with the similar ones in the literature. By using the following dimensionless quantities

$$\xi = \frac{x}{L}, \quad (\overline{U}, \overline{W}) = \frac{(u_0, w_0)}{h}, \quad \overline{N}_{x0} = \frac{N_{x0}}{A_{110}},$$
$$(\bar{I}_1, \bar{I}_2, \bar{I}_3) = \left(\frac{I_1}{I_{10}}, \frac{I_2}{I_{10}h}, \frac{I_3}{I_{10}h^2}\right), \quad \eta = \frac{L}{h}, \quad \psi = \Psi$$

$$(a_{11}, a_{55}, b_{11}, d_{11}) = \left(\frac{A_{11}}{A_{110}}, \frac{A_{55}}{A_{110}}, \frac{B_{11}}{A_{110}h}, \frac{D_{11}}{A_{110}h^2}\right),$$
$$\omega = \Omega L\sqrt{\frac{I_{10}}{A_{110}}}, \quad \tau = \frac{t}{L}\sqrt{\frac{A_{110}}{I_{10}}}, \quad k_1 = \frac{K_1 L^2}{A_{110}}, \quad k_2 = \frac{K_2}{A_{110}}$$

where A_{110} and I_{10} are the values of A_{11} and I_1 of a homogeneous beam made from pure matrix material, the governing Eq. (18) can be transformed into the following dimensionless form:

$$a_{11}\frac{\partial^2 \overline{U}}{\partial \xi^2} + b_{11}\frac{\partial^2 \psi}{\partial \zeta^2} = \bar{I}_1\frac{\partial^2 \overline{U}}{\partial \tau^2} + \bar{I}_2\frac{\partial^2 \psi}{\partial \tau^2}$$
$$\kappa a_{55}\left(\frac{\partial^2 \overline{W}}{\partial \zeta^2} + \eta\frac{\partial \psi}{\partial \zeta}\right) - k_1\overline{W} + k_2\frac{\partial^2 \overline{W}}{\partial \zeta^2} + \overline{N}_{x0}\frac{\partial^2 \overline{W}}{\partial \zeta^2} = \bar{I}_1\frac{\partial^2 \overline{W}}{\partial \tau^2},$$
$$b_{11}\frac{\partial^2 \overline{U}}{\partial \zeta^2} + d_{11}\frac{\partial^2 \psi}{\partial \zeta^2} - \kappa\eta a_{55}\left(\frac{\partial \overline{W}}{\partial \zeta} + \eta\psi\right) = \bar{I}_2\frac{\partial^2 \overline{U}}{\partial \tau^2} + \bar{I}_3\frac{\partial^2 \psi}{\partial \tau^2} \tag{20}$$

3.2. Generalized differential quadrature method (GDQM)

In this paper, the generalized differential quadrature method (GDQM) is used to solve the governing equations of CNTRC beams. According to GDQ method the rth-order partial derivative of a continuous function $f(\zeta)$ with respect to ζ at a given point ζ_i can be approximated as a linear sum of weighted function values at all of the discrete points in the domain of ζ i.e. [26,27]

$$\frac{\partial^r f(\zeta_i)}{\partial \zeta^r} = \sum_{k=1}^{N} c_{ik}^{(r)} f(\zeta_k), \quad i = 1, \ldots, N, r = 1, \ldots, N-1 \tag{21}$$

where N is the number of sampling points in the axial direction of the beam, $f(\zeta_k)$ represents the functional value at a sample point ζ_k, and $c_{ik}^{(r)}$ are the weighting coefficients of the rth-order derivative. The weighting coefficients for the first derivative (i.e. $r = 1$) are:

$$c_{ij}^{(1)} = \begin{cases} \dfrac{M^{(1)}(x_i)}{(x_i - x_j)M^{(1)}(x_j)} & i \neq j, \quad i,j = 1,2,\ldots,N \\ -\sum\limits_{j=1, i\neq j}^{N} c_{ij}^{(1)} & i = j, \quad i = 1,2,\ldots,N \end{cases} \tag{22}$$

where

$$M(x_i) = \prod_{j=1, i\neq j}^{N}(x_i - x_j) \tag{23}$$

For higher-order derivatives

$$c_{ij}^{(1)} = \begin{cases} r\left[c_{ii}^{(r-1)}c_{ij}^{(1)} - \dfrac{c_{ij}^{(r-1)}}{(x_i - x_j)}\right] & i\neq j,\ i,j=1,2,\ldots,N,\ r=2,3,\ldots,N-1 \\ -\sum\limits_{j=1, i\neq j}^{N} c_{ij}^{(r)} & i=j,\ i=1,2,\ldots,N \end{cases} \tag{24}$$

In the present study, the grid points are taken non-uniformly spaced and are given by the following equation:

$$\zeta_i = \frac{1}{2}\left(1 - \cos\left(\frac{i-1}{N-1}\pi\right)\right), \quad i = 1, 2, \ldots., N \tag{25}$$

3.3. Free vibration analysis

The dimensionless governing equations for free vibration of CNTRC beams can be obtained from Eq. (20) by eliminating the axial force ($N_{x0} = 0$). In harmonic vibration analysis, the displacements can be expressed as:

$$\begin{aligned}\overline{W}(x,t) &= w(x)e^{-i\omega t}\\ \overline{U}(x,t) &= u(x)e^{-i\omega t}\\ \psi(x,t) &= \Psi(x)e^{-i\omega t}\end{aligned} \tag{26}$$

where$i = \sqrt{-1}$ and ω is the dimensionless natural frequency. By substituting Eq. (26) into Eq. (20) and then applying the GDQ-rule expressed in Eqs. (22) and (24) at Eq. (20), the following relations are obtained:

$$\begin{aligned}&a_{11}\sum_{j=1}^{N}B_{ij}u_j + b_{11}\sum_{j=1}^{N}B_{ij}\Psi_j = -\bar{I}_1\omega^2 u_i - \bar{I}_2\omega^2\Psi_i\\ &\kappa a_{55}\left(\sum_{j=1}^{N}B_{ij}w_j + \sum_{j=1}^{N}A_{ij}\Psi_j\right) - k_1 w_i + k_2\sum_{j=1}^{N}B_{ij}w_j = -\bar{I}_1\omega^2 w_i\\ &b_{11}\sum_{j=1}^{N}B_{ij}u_j + d_{11}\sum_{j=1}^{N}B_{ij}\Psi_j - \kappa\eta a_{55}\left(\sum_{j=1}^{N}A_{ij}w_j + \eta\Psi_i\right)\\ &= -\bar{I}_2\omega^2 u_i - \bar{I}_3\omega^2\Psi_i\end{aligned} \tag{27}$$

where A_{ij} andB_{ij} are the first and second order GDQM weighting coefficients, respectively.

The associated boundary conditions can be handled in the same way. For example, the dimensionless boundary condition of clamped-free beams is

$$u_1 = w_1 = \Psi_1 = 0 \text{ at } \zeta = 0, \quad \begin{cases} N_x = a_{11}\sum_{j=1}^{N}A_{Nj}u_j + b_{11}\sum_{j=1}^{N}A_{Nj}\Psi_j = 0\\ M_x = b_{11}\sum_{j=1}^{N}A_{Nj}u_j + d_{11}\sum_{j=1}^{N}A_{Nj}\Psi_j = 0 \quad \text{at } \zeta = 1\\ Q_x = \kappa A_{55}\left(\sum_{j=1}^{N}A_{Nj}w_j + \eta\Psi_N\right) = 0\end{cases} \tag{28}$$

Implementing the boundary conditions into Eq. (27) leads to the following system of algebraic:

$$\begin{bmatrix}[S_{bb}] & [S_{bd}]\\ [S_{db}] & [S_{dd}]\end{bmatrix}\begin{Bmatrix}\{U_b\}\\ \{U_d\}\end{Bmatrix} = \omega^2\begin{bmatrix}[0] & [0]\\ [0] & [\bar{I}_i]\end{bmatrix}\begin{Bmatrix}\{U_b\}\\ \{U_d\}\end{Bmatrix} \tag{29}$$

where $\{U_d\}$ and $\{U_b\}$ are as follows:

$$\{U_b\} = \{\{u_b\},\{w_b\},\{\Psi_b\}\}^T,\ \{U_d\} = \{\{u_d\},\{w_d\},\{\Psi_d\}\}^T \tag{30}$$

in relation Eq. (30), subscripts '*b*' and '*d*' refer to the points at the boundary and in the interior domain respectively. $[\bar{I}_i]$ is dimensionless inertia terms matrices. Eliminating the boundary degrees of freedom, this equation becomes:

$$\left([S] - \omega^2[\bar{I}_i]\right)\{U_d\} = \{0\} \tag{31}$$

where

$$[S] = [S_{dd}] - [S_{db}][S_{bb}]^{-1}[S_{bd}] \tag{32}$$

The natural frequencies of the CNTRC beams considered can be determined by solving the standard eigenvalue problem Eq. (31).

3.4. Buckling of CNTRC beams

For CNTRC beams under axial compression *P*, the governing equations are derived from Eq. (20) by setting the inertia terms to zero and $\overline{N}_{x0} = -P$.

$$\begin{aligned}&a_{11}\frac{\partial^2\overline{U}}{\partial\xi^2} + b_{11}\frac{\partial^2\Psi}{\partial\zeta^2} = 0\\ &\kappa a_{55}\left(\frac{\partial^2\overline{W}}{\partial\zeta^2} + \eta\frac{\partial\Psi}{\partial\zeta}\right) - k_1\overline{W} + k_2\frac{\partial^2\overline{W}}{\partial\zeta^2} - P\frac{\partial^2\overline{W}}{\partial\zeta^2} = 0,\\ &b_{11}\frac{\partial^2\overline{U}}{\partial\zeta^2} + d_{11}\frac{\partial^2\Psi}{\partial\zeta^2} - \kappa\eta a_{55}\left(\frac{\partial\overline{W}}{\partial\zeta} + \eta\Psi\right) = 0\end{aligned} \tag{33}$$

Table 1
Convergence and accuracy of the dimensionless frequency parameters and critical buckling load FGM beams ($L/h = 6$, $E_2/E_1 = 5$).

	BC's	$N = 5$	$N = 7$	$N = 9$	$N = 11$	$N = 13$	Ref. [29].	Ref. [28]
Frequency								
$(k_w,k_s) = (0.00,0.00)$	H–H	0.4526	0.4599	0.4598	0.4598	0.4598	0.4597	0.4543
$(k_w,k_s) = (0.05,0.00)$		0.5509	0.5570	0.5568	0.5568	0.5568	0.5567	–
$(k_w,k_s) = (0.05,0.01)$		0.7053	0.7107	0.7105	0.7105	0.7105	0.7103	–
$(k_w,k_s) = (0.00,0.00)$	C–F	0.1486	0.1557	0.1556	0.1556	0.1556	0.1556	0.1547
$(k_w,k_s) = (0.05,0.00)$		0.3490	0.3521	0.3520	0.3520	0.3520	0.3520	–
$(k_w,k_s) = (0.05,0.01)$		0.3473	0.3370	0.3367	0.3367	0.3367	0.3367	–
$(k_w,k_s) = (0.00,0.00)$	C–C	0.8662	0.8598	0.8600	0.8600	0.8600	0.8600	0.8494
$(k_w,k_s) = (0.05,0.00)$		0.9218	0.9157	0.9159	0.9159	0.9159	0.9159	–
$(k_w,k_s) = (0.05,0.01)$		1.0267	1.0292	1.0293	1.0293	1.0293	1.0293	–
Buckling								
$(k_w,k_s) = (0.00,0.00)$	H–H	0.052801	0.054305	0.054256	0.054256	0.054256	–	0.054256
	C–F	0.011747	0.012312	0.012308	0.012308	0.012308	–	0.012588
	C–C	0.180381	0.155643	0.155542	0.155536	0.155536	–	0.155540

Similar to free vibration analysis, by applying the GDQM rule expressed in Eqs. (22) and (24) into Eq. (33), the following relations are obtained:

$$\begin{aligned} &a_{11}\sum_{j=1}^{N}B_{ij}u_j+b_{11}\sum_{j=1}^{N}B_{ij}\Psi_j=0\\ &\kappa a_{55}\left(\sum_{j=1}^{N}B_{ij}w_j+\sum_{j=1}^{N}A_{ij}\Psi_j\right)-k_1w_i+k_2\sum_{j=1}^{N}B_{ij}w_j-P\sum_{j=1}^{N}B_{ij}w_j=0\\ &b_{11}\sum_{j=1}^{N}B_{ij}u_j+d_{11}\sum_{j=1}^{N}B_{ij}\Psi_j-\kappa\eta a_{55}\left(\sum_{j=1}^{N}A_{ij}w_j+\eta\Psi_i\right)=0 \end{aligned} \tag{34}$$

Combination of Eq. (34) with the boundary conditions gives the following system of linear equations:

$$\begin{bmatrix}[S_{bb}] & [S_{bd}]\\ [S_{db}] & [S_{dd}]\end{bmatrix}\begin{Bmatrix}\{U_b\}\\ \{U_d\}\end{Bmatrix}=P\begin{bmatrix}[0] & [0]\\ [A_{db}] & [A_{dd}]\end{bmatrix}\begin{Bmatrix}\{U_b\}\\ \{U_d\}\end{Bmatrix} \tag{35}$$

in relation Eq. (35), subscripts '*d*' and '*b*' refer to the points at the boundary and in the interior domain, respectively and *P* represent the buckling load.

After implementation of the boundary conditions, Eq. (35) can be written in matrix form as

$$([S]-P[A])\{U_d\}=\{0\} \tag{36}$$

where

$$[S]=[S_{dd}]-[S_{db}][S_{bb}]^{-1}[S_{bd}]$$

$$[A]=[A_{dd}]-[A_{db}][S_{bb}]^{-1}[S_{bd}]$$

Clearly, the lowest positive solution of Eq. (36) gives the critical buckling load P_{cr}.

4. Numerical results and discussion

First, in order to confirm the proficiency of the present method, free vibration and buckling analysis of FG beams with and without elastic foundation and different boundary conditions are investigated. For this purpose the numerical results of free vibration and buckling analysis CNTRC beams are presented.

Table 1 presents the dimensionless frequency as well as critical buckling load of FG beam with different boundary conditions. The results are compared with similar ones in the literature. As observed there is good agreement between the results. The convergence study of the results is listed in Table 1 too. As noticed, fast rate of convergence of the method is evident and it is found that only 9 grid points in the thickness direction can yield accurate results. Hence, $N = 9$ is used in all of the following numerical calculations.

Table 2
Comparisons of dimensionless frequency parameters $\omega = \Omega L\sqrt{I_{10}/A_{110}}$ CNTRC beams ($L/h = 10$).

$V^*_{cnt} = 12$	UD		FG-Λ		FG-X	
	Present	Ref. [21].	Present	Ref. [21].	Present	Ref. [23].
H–H	1.2581	1.2576	1.2300	1.2296	1.3859	1.3852
C–H	1.4565	1.4556	1.3951	1.3944	1.5394	1.5385
C–C	1.6691	1.6678	1.6073	1.6063	1.7242	1.7230

The material properties of FG beams are : $E_1 = 70$ GPa, $\nu_1 = 0.33$, $\frac{E_2}{E_1} = 5$, $\rho_1 = 2780$ kg/m^3, $L/h = 6$ where E_1 and E_2 denote Young's modulus at the top and bottom surfaces of the beam, respectively.

4.1. Free vibration analysis of CNTRC beams

First, the effective material properties of CNTRCs are determined. Poly methyl methacrylate, referred to PMMA, is considered as the matrix, the material properties are assumed to be $\upsilon^m = 0.3$, $\rho^m = 1190$ kg/m^3,$E^m = 2.5$ Gpa at room temperature (300 K). The armchair (10,10) SWCNTs are selected as reinforcements with $\upsilon^{cnt} = 0.19, G^{cnt}_{12} = 17.2Gpa, E^{cnt}_{11} = 600Gpa \;\; E^{cnt}_{22} = 10Gpa,$ $\rho^{cnt} = 1400$ kg/m^3.

The CNT efficiency parameters introduced in Eqs. (1a) and (1b) are estimated by matching the Young's moduli E_{11} and E_{22} of CNTRCs predicted from the rule of mixture to those from the MD simulations given by Han and Elliott. For example $\eta_1 = 1.2833$ and $\eta_2 = 1.0556$ for the case of $V^*_{cnt} = 0.12$, and $\eta_1 = 1.3414$ and $\eta_2 = 1.7101$ for the case of $V^*_{cnt} = 0.17$, and $\eta_1 = 1.3238$ and $\eta_2 = 1.7380$ for the case of $V^*_{cnt} = 0.28$. In addition, it is assumed that $\eta_3 = \eta_2$. These values will be used in all the following examples.

Table 2 lists the dimensionless fundamental frequency of CNTRC beams, for various boundary conditions ($L/h = 10$). Again, it can be observed that there is a very good agreement between the results.

In Tables 3–6, the effects of the elastic foundation coefficients as well as different values of CNT volume fraction $V^*_{cnt} = (0.12, 0.17, 0.28)$ on the first three dimensionless fundamental frequency parameters$\omega = \Omega L\sqrt{I_{10}/A_{110}}$ of various types of CNTRC beams are shown for different boundary conditions including hinged–hinged, clamped-hinged, clamped–clamped and clamped-free. Two foundation models are considered. The stiffness parameters are $(k_w, k_s) = (0.1, 0.02)$ for the Pasternak elastic foundation, $(k_w, k_s) = (0.1, 0.00)$ for the Winkler elastic foundation and

Table 3
First three dimensionless natural frequency $\omega = \Omega L\sqrt{I_{10}/A_{110}}$ of (H–H) CNTRC beams ($L/h = 15$).

V^*_{cnt}		$(k_w,k_s) = (0.00, 0.00)$			$(k_w,k_s) = (0.1, 0.00)$			$(k_w,k_s) = (0.1, 0.02)$		
		ω_1	ω_2	ω_3	ω_1	ω_2	ω_3	ω_1	ω_2	ω_3
0.12	UD	0.9753	2.8728	4.8704	1.0241	2.8898	4.8804	1.1144	3.0203	5.0552
	FG-Λ	0.9453	2.6424	4.6675	0.9957	2.6607	4.6780	1.0883	2.8013	4.8596
	FG-◇	0.7527	2.4562	4.4320	0.8150	2.4760	4.4430	0.9258	2.6268	4.6338
	FG-X	1.1150	3.0814	5.0695	1.1581	3.0972	5.0791	1.2386	3.2194	5.2474
0.17	UD	1.1999	3.6276	6.2363	1.2396	3.6409	6.2441	1.3145	3.7444	6.3804
	FG-Λ	1.1609	3.3084	5.9498	1.2019	3.3229	5.9579	1.2790	3.4354	6.1002
	FG-◇	0.9155	3.0577	5.6139	0.9670	3.0734	5.6225	1.0612	3.1951	5.7731
	FG-X	1.3830	3.9293	6.5447	1.4176	3.9416	6.5521	1.4836	4.0375	6.6822
0.28	UD	1.4401	4.1362	6.9245	1.4728	4.1477	6.9314	1.5352	4.2372	7.0523
	FG-Λ	1.4027	3.8639	6.7618	1.4362	3.8762	6.7688	1.5002	3.9714	6.8923
	FG-◇	1.1202	3.6056	6.4434	1.1619	3.6187	6.4508	1.2400	3.7208	6.5802
	FG-X	1.6493	4.4752	7.3068	1.6779	4.4858	7.3133	1.7330	4.5688	7.4280

Table 4
First three dimensionless natural frequencies of (C–H) CNTRC beams ($L/h = 15$).

V^*_{cnt}		$(k_w, k_s) = (0.00, 0.00)$			$(k_w, k_s) = (0.1, 0.00)$			$(k_w, k_s) = (0.1, 0.02)$		
		ω_1	ω_2	ω_3	ω_1	ω_2	ω_3	ω_1	ω_2	ω_3
0.12	UD	1.2444	3.0159	4.9342	1.2831	3.0321	4.9441	1.3586	3.1565	5.1165
	FG-Λ	1.1529	2.8472	4.7474	1.1945	2.8643	4.7577	1.2762	2.9957	4.9361
	FG-◇	1.0331	2.6814	4.5619	1.0794	2.6995	4.5726	1.1705	2.8389	4.7579
	FG-X	1.3577	3.1817	5.1092	1.3932	3.1970	5.1188	1.4622	3.3153	5.2857
0.17	UD	1.5602	3.8402	6.3370	1.5910	3.8528	6.3446	1.6523	3.9504	6.4782
	FG-Λ	1.4344	3.6064	6.0765	1.4678	3.6198	6.0844	1.5349	3.7235	6.2232
	FG-◇	1.2769	3.3772	5.8126	1.3143	3.3915	5.8209	1.3902	3.5025	5.9659
	FG-X	1.7188	4.0843	6.6094	1.7467	4.0961	6.6168	1.8020	4.1880	6.7451
0.28	UD	1.8040	4.3112	6.9987	1.8302	4.3222	7.0055	1.8822	4.4081	7.1251
	FG-Λ	1.6933	4.1393	6.8633	1.7212	4.1507	6.8702	1.7772	4.2400	6.9917
	FG-◇	1.5229	3.9112	6.6127	1.5538	3.9233	6.6199	1.6166	4.0178	6.7459
	FG-X	1.9813	4.6030	7.3560	2.0052	4.6133	7.3624	2.0523	4.6939	7.4764

Table 5
First three dimensionless natural frequencies $\omega = \Omega L\sqrt{I_{10}/A_{110}}$ of (C–C) CNTRC beams ($L/h = 15$).

V^*_{cnt}		$(k_w, k_s) = (0.00, 0.00)$			$(k_w, k_s) = (0.1, 0.00)$			$(k_w, k_s) = (0.1, 0.02)$		
		ω_1	ω_2	ω_3	ω_1	ω_2	ω_3	ω_1	ω_2	ω_3
0.12	UD	1.5085	3.1353	4.9979	1.5406	3.1508	5.0077	1.6038	3.2714	5.1779
	FG-Λ	1.4068	2.9997	4.8363	1.4412	3.0159	4.8464	1.5096	3.1420	5.0216
	FG-◇	1.3180	2.8762	4.6840	1.3546	2.8931	4.6944	1.4282	3.0249	4.8750
	FG-X	1.6000	3.2629	5.1514	1.6303	3.2778	5.1609	1.6895	3.3937	5.3264
0.17	UD	1.9144	4.0187	6.4348	1.9396	4.0307	6.4423	1.9901	4.1250	6.5742
	FG-Λ	1.7721	3.8312	6.2139	1.7993	3.8438	6.2216	1.8546	3.9429	6.3578
	FG-◇	1.6500	3.6565	5.9970	1.6791	3.6697	6.0051	1.7393	3.7740	6.1460
	FG-X	2.0498	4.2111	6.6753	2.0733	4.2226	6.6825	2.1200	4.3124	6.8100
0.28	UD	2.1618	4.4556	7.0745	2.1837	4.4663	7.0812	2.2274	4.5498	7.1994
	FG-Λ	2.0504	4.3414	6.9783	2.0735	4.3524	6.9851	2.1202	4.4382	7.1046
	FG-◇	1.9284	4.1740	6.7728	1.9530	4.1854	6.7798	2.0032	4.2750	6.9028
	FG-X	2.3169	4.7051	7.4093	2.3374	4.7152	7.4157	2.3779	4.7943	7.5288

$(k_w, k_s) = (0.00, 0.00)$ for the beams without any elastic foundation. As noticed both Winkler and Pasternak elastic coefficients lead to increase the dimensionless fundamental frequency parameters under various boundary conditions. It can also be seen the dimensionless fundamental frequency parameters increase with increasing in the volume fraction of CNTs (V^*_{cnt}). It is noticeable the lowest frequency parameter is obtained by using FG-◇ CNTRC volume fractions profile. On the contrary, oriented, straight CNTs with FG-X CNTRC profile have the maximum value of the frequency parameter. Therefore, graded CNTs volume fractions with symmetric distributions through the beam thickness have higher capabilities to reduce or increase the frequency parameter as compared with uniformly and asymmetric distributions.

It should be mentioned that the UD-CNTRC and FG-CNTRC beams have the same mass fraction of CNT. Additionally, the resulting frequency changes due to boundary condition such that the highest frequencies are obtained for the C–C beams, followed by C–H and H–H beams respectively and the C–F beam has the lowest fundamental frequency at every volume fraction. For all types of beams except the cantilever ones, the fundamental frequency is higher when resting on a Pasternak foundation than on a Winkler foundation.

Fig. 3 shows fundamental frequency parameter, ω_1, of different CNTs distributions with $(k_w, k_s) = (0.1, 0.02)$ and $V^*_{cnt} = 0.28$ versus slenderness ratio. It can be inferred from Fig. 3 that frequency of FG-X CNTRC beams are higher than those of beams with other CNTs distributions. Hence, in the following figures only UD-CNTRC beam and FG-CNTRC beam of Type X are considered. Also one can see, the frequency parameter decreases for all types of distribution with increasing the slenderness ratios.

Table 6
First three dimensionless natural frequencies $\omega = \Omega L\sqrt{I_{10}/A_{110}}$ of (C–F) CNTRC beams ($L/h = 15$).

V^*_{cnt}		$(k_w, k_s) = (0.00, 0.00)$			$(k_w, k_s) = (0.1, 0.00)$			$(k_w, k_s) = (0.1, 0.02)$		
		ω_1	ω_2	ω_3	ω_1	ω_2	ω_3	ω_1	ω_2	ω_3
0.12	UD	0.3764	1.7006	3.6648	0.4893	1.7290	3.6781	0.4825	1.8115	3.8143
	FG-Λ	0.3193	1.5473	3.4380	0.4469	1.5784	3.4521	0.4368	1.6652	3.5922
	FG-◇	0.2809	1.4266	3.2489	0.4203	1.4603	3.2638	0.4083	1.5520	3.4090
	FG-X	0.4416	1.8497	3.8777	0.5411	1.8759	3.8902	0.5380	1.9549	4.0229
0.17	UD	0.4587	2.1365	4.6614	0.5544	2.1590	4.6718	0.5471	2.2242	4.7775
	FG-Λ	0.3866	1.9287	4.3500	0.4963	1.9535	4.3610	0.4860	2.0230	4.4703
	FG-◇	0.3394	1.7685	4.0913	0.4606	1.7956	4.1030	0.4483	1.8698	4.2171
	FG-X	0.5413	2.3437	4.9706	0.6245	2.3642	4.9803	0.6203	2.4260	5.0825
0.28	UD	0.5612	2.4614	5.2446	0.6404	2.4806	5.2536	0.6359	2.5381	5.3483
	FG-Λ	0.4761	2.2685	5.0007	0.5673	2.2893	5.0102	0.5595	2.3491	5.1059
	FG-◇	0.4197	2.0993	4.7399	0.5209	2.1217	4.7499	0.5110	2.1849	4.8489
	FG-X	0.6586	2.6987	5.6150	0.7273	2.7162	5.6235	0.7256	2.7705	5.7143

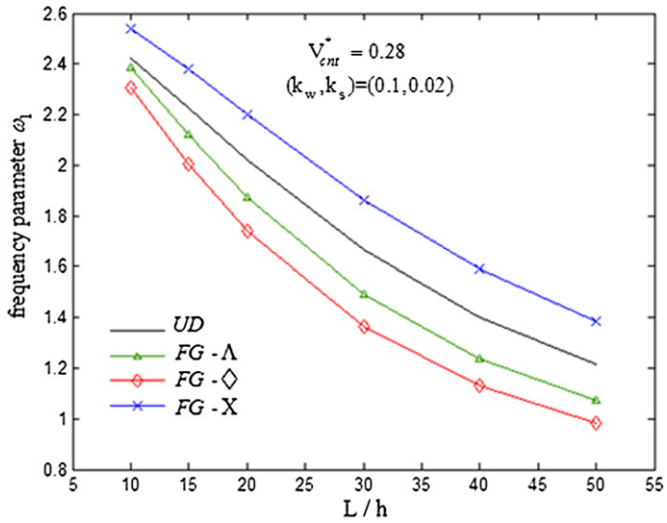

Fig. 3. Effect of the slenderness ratio on the fundamental frequency of four types of C–C. CNTRC beams on a Pasternak elastic foundation.

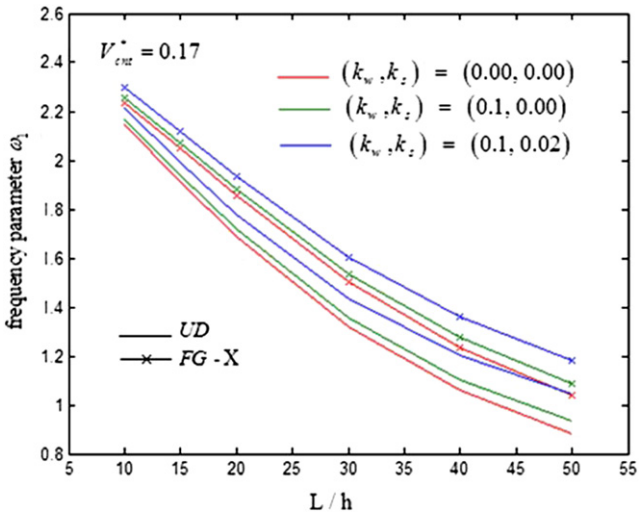

Fig. 5. Effect of foundation stiffness on the frequency of C–C CNTRC beams.

The variation of frequency of the nanocomposite beams with L/h ratios is shown in Fig. 4 for different CNT volume fraction. It can be noticed although the frequencies for the beams with FG-X and uniform distribution of CNTs decrease with the increase of the L/h ratio, but increase with increasing in the CNTs volume fraction V^*_{cnt}.

Fig. 5 illustrates the effect of the foundation stiffness on the frequency of CNTRC beams. As observed, the frequency parameter is increased with the increase of foundation stiffness for both UD and FG-X CNTRC beams.

Fig. 6 shows effect of the boundary conditions on the vibration behavior of CNTRC beam resting on Pasternak foundation. It can be concluded the C–C beams have the highest frequencies and on the contrary the C–F beams have the lowest fundamental frequencies.

4.2. Buckling analysis of CNTRC beams

In this section, numerical results of buckling analysis of CNTRC beams are presented. The material and geometric properties are the same as those for free vibration analyses. Tables 7–10 show effects of the elastic foundation coefficients and different values of CNT volume fraction on the dimensionless critical buckling load of various types of CNTRC beams for different boundary conditions.

It can be seen that among the four boundary conditions considered, the clamped-free beam has the minimum values while the clamped–clamped beam has the maximum values of critical buckling load. It is intelligible that the critical buckling load of FG-X CNTRC beam is larger among these four types of beams. It is also observed, the buckling load of the beams increases when resting on elastic foundation. It should be mentioned that the effects of k_s on the critical buckling load are more significant than those of k_w. It is also noticed the critical buckling load for all types of CNT distribution and different boundary conditions increases with the increase of the CNT volume fraction value.

In Table 11 the critical buckling load of different types of CNT distribution is given for V^*_{cnt} = 0.28. The foundation stiffness parameters are taken to be (k_w, k_s) = (0.1,0.02). According to this table, increasing the slenderness ratio led to buckling load reduction for each distribution. Also it is observed the FG-X distribution has the highest critical load.

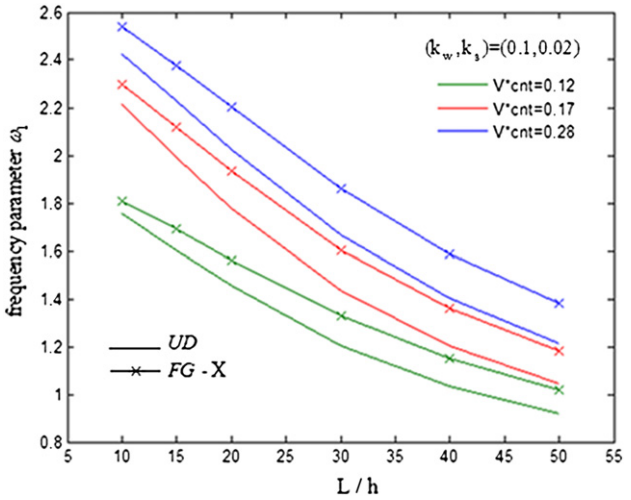

Fig. 4. Effect of CNT volume fraction on the fundamental frequency of C–C. CNTRC beams resting on a Pasternak elastic foundation.

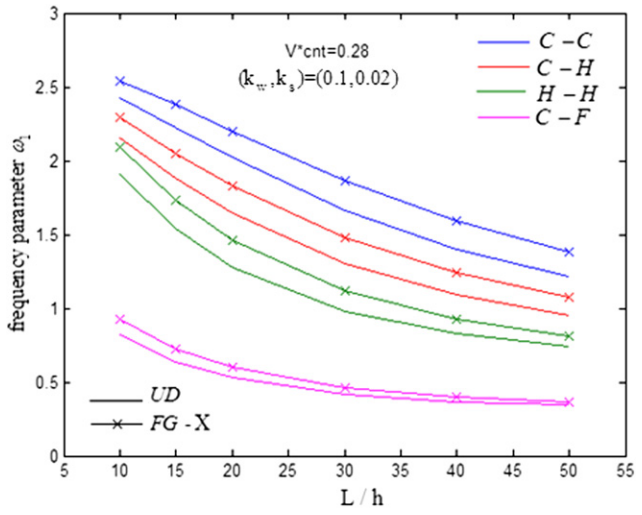

Fig. 6. Variation of the 1st frequency versus slenderness ratio at volume fraction 0.12.

Table 7
Dimensionless buckling load of (H–H) CNTRC beams ($L/h = 15$).

	V^*_{cnt}	UD	FG-Λ	FG-◇	FG-X
$(k_w, k_s) = (0.00, 0.00)$	0.12	0.098597	0.092530	0.058770	0.128833
	0.17	0.150559	0.140748	0.087704	0.199945
	0.28	0.220904	0.209323	0.133755	0.289646
$(k_w, k_s) = (0.1, 0.00)$	0.12	0.108729	0.102641	0.0689026	0.138965
	0.17	0.160697	0.150858	0.0978362	0.210077
	0.28	0.231036	0.219433	0.143887	0.299774
$(k_w, k_s) = (0.1, 0.02)$	0.12	0.128729	0.122641	0.088903	0.158965
	0.17	0.180692	0.170858	0.117836	0.230077
	0.28	0.251036	0.239433	0.163887	0.319774

Table 8
Dimensionless buckling load of (C–H) CNTRC beams ($L/h = 15$).

	V^*_{cnt}	UD	FG-Λ	FG-◇	FG-X
$(k_w, k_s) = (0.00, 0.00)$	0.12	0.149484	0.126376	0.099567	0.181451
	0.17	0.2349942	0.1956625	0.1521840	0.2908679
	0.28	0.3253990	0.2815180	0.2233645	0.3991979
$(k_w, k_s) = (0.1, 0.00)$	0.12	0.1582075	0.1349723	0.1080482	0.1903661
	0.17	0.2436821	0.2042408	0.1606523	0.2997283
	0.28	0.3342330	0.2901868	0.2319158	0.4082148
$(k_w, k_s) = (0.1, 0.02)$	0.12	0.1782075	0.1549723	0.1280482	0 0.2103661
	0.17	0.2636821	0.2242408	0.1806523	0.3197283
	0.28	0.3542330	0.3101868	0.2519158	0.4282148

Table 9
Dimensionless buckling load of (C–C) CNTRC beams ($L/h = 15$).

	V^*_{cnt}	UD	FG-Λ	FG-◇	FG-X
$(k_w, k_s) = (0.00, 0.00)$	0.12	0.213958	0.181823	0.156758	0.245934
	0.17	0.344251	0.287861	0.245191	0.403501
	0.28	0.455602	0.399275	0.346965	0.532998
$(k_w, k_s) = (0.1, 0.00)$	0.12	0.221398	0.189291	0.164233	0.253333
	0.17	0.351801	0.295413	0.252742	0.411045
	0.28	0.463117	0.406809	0.354506	0.540496
$(k_w, k_s) = (0.1, 0.02)$	0.12	0.241398	0.209291	0.184233	0.273333
	0.17	0.371800	0.315413	0.272742	0.431045
	0.28	0.483117	0.426809	0.374506	0.560496

Table 10
Dimensionless buckling load of (C–F) CNTRC beams (L/$h = 15$).

	V^*_{cnt}	UD	FG-Λ	FG-◇	FG-X
$(k_w, k_s) = (0.00, 0.00)$	0.12	0.031234	0.021985	0.016790	0.044355
	0.17	0.046318	0.032234	0.024572	0.066253
	0.28	0.072178	0.050475	0.038680	0.102480
$(k_w, k_s) = (0.1, 0.00)$	0.12	0.047542	0.037938	0.032359	0.060903
	0.17	0.063385	0.049039	0 0.041095	0.083504
	0.28	0.089557	0.067717	0.055745	0.119989
$(k_w, k_s) = (0.1, 0.02)$	0.12	0.041901	0.032373	0.026890	0.055221
	0.17	0.057736	0.043415	0.035508	0.077847
	0.28	0.083912	0.062080	0.050117	0.114348

Table 11
Dimensionless buckling load of (H–H) CNTRC beams (k_w, k_s) = (0.1, 0.02), $V^*_{cnt} = 0.28$.

L/h	UD	FG-Λ	FG-◇	FG-X
10	0.387342	0.378099	0.275637	0.467794
15	0.251036	0.239433	0.163887	0.319774
20	0.174117	0.164475	0.111827	0.226701
30	0.102310	0.096524	0.068812	0.132612
40	0.072635	0.068994	0.052399	0.091493

5. Conclusions

In this paper, based on the Timoshenko beam theory, the free vibrations and buckling of nanocomposite beams reinforced by single-walled carbon nanotubes resting on an elastic foundation have been studied. The equations of motion have been determined through the Hamilton's principle. Generalized differential quadrature method is employed to obtain the natural frequency and critical buckling load of CNTRC beams with or without an elastic foundation for various boundary conditions. The material properties have been estimated though the rule of mixture. The numerical results reveal that the distribution of CNT, foundation stiffness and volume fraction of CNT have significant effects on the natural frequencies and critical buckling load of the CNTRC beams. The obtained results show the beams with FG-X distribution have higher fundamental frequency as well as critical buckling load in comparison with other distributions. As simple analysis the cross sectional geometry of the CNT/PMMA composite beam can be used to predict which beams will have the highest stiffness/resistance to bending and buckling, by considering the second moment of area. The 'X' distribution is the closest to an I-beam geometry, which has a higher moment of inertia compared with the other geometries Also it results both the natural frequency and the critical buckling load increase with using an elastic foundation or increasing CNT volume fraction.

The investigation on the effect of boundary conditions reveals the C–C beam has the greatest natural frequency and critical buckling load which is followed with C–H, H–H and then C–F respectively. It is worth noting that the natural frequencies and critical buckling loads decrease with increasing the slenderness ratio.

References

[1] Lau KT, Gu C, Gao GH, Ling HY, Reid SR. Stretching process of single- and multiwalled carbon nanotubes for nanocomposite applications. Carbon 2004; 42:426–8.
[2] Esawi AMK, Farag MM. Carbon nanotube reinforced composites: potential and current challenges. Mater Des 2007;28:2394–401.
[3] Salvetat D, Rubio A. Mechanical properties of carbon nanotubes: a fiber digest for beginners. Carbon 2002;40:1729–34.
[4] Fiedler B, Gojny FH, Wichmann MHG, Nolte MCM, Schulte K. Fundamental aspects of nano-reinforced composites. Compos Sci Technol 2006;66: 3115–25.
[5] Hu N, Fukunaga H, Lu C, Kameyama M, Yan B. Prediction of elastic properties of carbon nanotube reinforced composites. Proc Royal Soc A 2005;461: 1685–710.
[6] Han Y, Elliott J. Molecular dynamics simulations of the elastic properties of polymer/carbon nanotube composites. Comput Mater Sci 2007;39:315–23.
[7] Wan H, Delale F, Shen L. Effect of CNT length and CNT-matrix interphase in carbon nanotube (CNT) reinforced composites. Mech Res Commun 2005;32: 481–9.
[8] Wuite J, Adali S. Deflection and stress behaviour of nanocomposite reinforced beams using a multiscale analysis. Compos Struct 2005;71:388–96.
[9] Vodenitcharova T, Zhang LC. Bending and local buckling of a nanocomposite beam reinforced by a single-walled carbon nanotube. Int J Solids Struct 2006; 43:3006–24.
[10] Seidel GD, Lagoudas DC. Micromechanical analysis of the effective elastic properties of carbon nanotube reinforced composites. Mech Mater 2006;38: 884–907.
[11] Qian D, Dickey EC, Andrews R, Rantell T. Load transfer and deformation mechanisms in carbon nanotube–polystyrene composites. Appl Phys Lett 2000;76:2868–70.
[12] Shen HS. Nonlinear bending of functionally graded carbon nanotube reinforced composite plates in thermal environments. Compos Struc 2009;91: 9–19.
[13] Suresh S, Mortensen A. Fundamentals of functionally graded materials: processing and thermomechanical behavior of graded metals and metal ceramic composites. London: IOM Communications Ltd.; 1998.
[14] Shahba A, Rajasekaran S. Free vibration and stability of tapered Euler-Bernoulli beams made of axially functionally graded materials. Appl Math Model 2012;36:3094–111.

[15] watteanasakulpong Nuttawit, Gangadhara prusty B, kelly Donald W, Hoffman Mark. Free vibration analysis of layered functionally graded beams with experimental validation. Mater & Des 2012;36:182–90.
[16] Shen HS, Zhang CL. Thermal buckling and postbuckling behavior of functionally graded carbon nanotube-reinforced composite plates. Mater & Des 2010;31:3403–11.
[17] Wang ZX, Shen HS. Nonlinear vibration of nanotube-reinforced composite plates in thermal environments. Comput Mater Sci 2011;50:2319–30.
[18] Wang ZX, Shen HS. Nonlinear vibration and bending of sandwich plates with nanotube-reinforced composite face sheets. Compos Part B –Eng 2012;43: 411–21.
[19] Zhu Ping, Lei ZX, Liew KM. Static and free vibration analyses of carbon nanotube-reinforced composite plates using finite element method with first order shear deformation plate theory. Compos Struct 2012;94: 1450–60.
[20] Shen HS. Postbuckling of nanotube-reinforced composite cylindrical shells in thermal environments. Part I: axially-loaded shells. Compos Struct 2011;93: 2096–108.
[21] Shen HS. Postbuckling of nanotube-reinforced composite cylindrical shells in thermal environments. Part II: pressure-loaded shells. Compos Struct 2011; 93:2496–503.
[22] Shen HS, Xiang Y. Nonlinear vibration of nanotube-reinforced composite cylindrical shells in thermal environments. Comput Methods Appl Mech Engrg 2012;213:196–205.
[23] Ke LL, Yang J, Kitipornchai S. Nonlinear free vibration of functionally graded carbon nanotube-reinforced composite beams. Compos Struct 2010;92:676–83.
[24] Yas MH, Heshmati M. Dynamic analysis of functionally graded nanocomposite beams reinforced by randomly oriented carbon nanotube under the action of moving load. Appl Math Model 2012;36:1371–94.
[25] Reddy JN. Mechanics of laminated composite plates and shells: theory and analysis. Boca Raton: FL: CRC Press; 2004.
[26] Shu C. Differential quadrature and its application in engineering. New York: Springer Publication; 2000.
[27] Shu C, Du H. Implementation of clamped and simply supported boundary conditions in the GDQ free vibration analysis of beams and plates. J Sound Vib 1997;34:819–35.
[28] Ke LL, Yang J, Kitipornchai S, Xiang Y. Flexural vibration and elastic buckling of a cracked Timoshenko beam made of functionally graded materials. Mech Adv Mater Struct 2008;16:488–502.
[29] Yan T, Kitipornchai S, Yang J, He Qiao. Dynamic behaviour of edge-cracked shear deformable functionally graded beams on an elastic foundation under a moving load. Compos Structs 2011;93:2992–3001.